sustainability

MDPI

Article

Optimizing Freight Vehicle Routing in Dynamic Time-Varying Networks with Carbon Dioxide Emission Trajectory Analysis

Rui Song [1,*], Wanen Qin [1], Wen Shi [1] and Xingjian Xue [2]

[1] School of Logistics and Transportation, Central South University of Forestry and Technology, Changsha 410004, China; 20221100305@csuft.edu.cn (W.Q.); 20221200311@csuft.edu.cn (W.S.)
[2] School of Landscape Architecture, Central South University of Forestry and Technology, Changsha 410004, China; t20110781@csuft.edu.cn
* Correspondence: t20162295@csuft.edu.cn

Abstract: In this study, we formulate a freight vehicle path-planning model in the context of dynamic time-varying networks that aims to capture the spatial and temporal distribution characteristics inherent in the carbon dioxide emission trajectories of freight vehicles. Central to this model is the minimization of total carbon dioxide emissions from vehicle distribution, based on the comprehensive modal emission model (CMEM). Our model also employs the freight vehicle travel time discretization technique and the dynamic time-varying multi-path selection strategy. We then design an improved genetic algorithm to solve this complicated problem. Empirical results vividly illustrate the superior performance of our model over alternative objective function models. In addition, our observations highlight the central role of accurate period partitioning in time segmentation considerations. Finally, the experimental results underline that our multi-path model is able to detect the imprint of holiday-related effects on the spatial and temporal distribution of carbon dioxide emission trajectories, especially when compared to traditional single-path models.

Keywords: carbon dioxide emissions; trajectory characteristics; dynamic VRP; multi-path selection

check for updates

Citation: Song, R.; Qin, W.; Shi, W.; Xue, X. Optimizing Freight Vehicle Routing in Dynamic Time-Varying Networks with Carbon Dioxide Emission Trajectory Analysis. *Sustainability* **2023**, *15*, 15504. https://doi.org/10.3390/su152115504

Academic Editor: Jack Barkenbus

Received: 18 September 2023
Revised: 30 October 2023
Accepted: 30 October 2023
Published: 31 October 2023

Copyright: © 2023 by the authors. Licensee MDPI, Basel, Switzerland. This article is an open access article distributed under the terms and conditions of the Creative Commons Attribution (CC BY) license (https://creativecommons.org/licenses/by/4.0/).

1. Introduction

The ongoing process of urbanization and increasing population density has led to a significant increase in vehicle emissions, making them a major contributor to air pollution and carbon dioxide emissions in Chinese cities. This trend poses significant health and disease risks to the inhabitants of these urban areas. In 2019, CO_2 emissions from road transport in China accounted for approximately 7.9% of the country's total emissions [1], making it the third largest contributor of emissions only after the energy supply and industrial production sectors. Moreover, the transport sector has experienced the fastest growth in carbon dioxide emissions in recent times. A distinguishing feature of carbon dioxide emissions from road transport, as opposed to those from fixed industrial sources, is their complex, random, and dynamically variable nature [2]. This inherent complexity poses a significant challenge to the accurate quantification of the carbon dioxide emissions associated with road transport, warranting dedicated research efforts to fill this knowledge gap.

In passenger transport, the promotion of new energy vehicles holds great promise in reducing tailpipe emissions, improving urban air quality, protecting the environment, and contributing to global climate change mitigation efforts. However, in freight transport, with increasing congestion on urban roads and rapidly growing demand for freight distribution, logistics companies need to rationally design the optimal vehicle distribution plan to minimize the impact of carbon dioxide emissions from freight vehicles on the urban environment [3]. How to let freight vehicles meet the goal of low-carbon transport, make full use of the dynamic time-varying characteristics of the urban road network, effectively avoid congested roads, and find the best distribution route scheme is still a very important vehicle route optimization problem.

The vehicle route problem (VRP) is a prominent and challenging topic within the field of transportation [4]. Theoretically, the VRP falls within the NP-hard problem domains, known for their computational complexity [5,6]. The practical manifestation of this problem is exacerbated by a variety of complex constraints encountered in real-world vehicle distribution scenarios. These complexities contribute to the significant size of the problem and make the search for accurate and precise solutions extremely challenging. Our research focuses on two interrelated topics: the green vehicle routing problem (green VRP) and the dynamic vehicle routing problem (dynamic VRP). The green VRP involves designing an optimal vehicle path distribution scheme that minimizes fuel consumption or tailpipe emissions [7]. On the other hand, dynamic VRP revolves around incorporating the real-time dynamics of the road network [8].

As many countries and cities pay more attention to urban carbon dioxide emissions and air pollution, green VRP has become one of the popular directions in VRP research. The research mainly focuses on the pollution-routing problem, energy-minimizing VRP, fuel consumption in VRP, etc. [9–11]. The underlying constructs of these problems invariably focus on minimizing fuel consumption or mitigating carbon dioxide emissions caused by vehicle movements. To illustrate, the work of [12] introduces a dual-objective framework for green vehicle routing that converges on the twin goals of reducing overall carbon dioxide emissions and reducing operational costs. Li et al. [13] maximize the vehicle distribution revenue and minimize the fuel consumption cost by designing the multi-destination green vehicle path problem (MDGVRP). Anjum et al. [14] provide a distinctive bi-objective paradigm by designing a planning framework for the green VRP. In the field of solution methodologies, two types of algorithms have been introduced: exact algorithms and intelligent heuristic algorithms. The former, exact algorithms, generate a construct based on mixed integer programming with the explicit purpose of deriving optimal solutions [15,16]. However, as the size of the problem increases, the computational effort grows exponentially, making them more suitable for small-scale optimization problems [17]. Conversely, intelligent heuristic algorithms cannot be compared with exact algorithms in terms of solution accuracy, but, when solving large-scale problems, they can find suboptimal or satisfactory solutions to the problems within a limited time, and are widely used in practical work [18–21].

Dynamic VRP emphasizes the dynamic nature of urban roadways and traffic environments; i.e., as road traffic changes in real time, the routes of delivery vehicles need to be flexibly selected. Specifically, Huang et al. [22] combine route flexibility with the time-dependent travel time by adopting a route path selection method. Zhao et al. [23] propose a model to obtain the time-dependent travel time based on historical traffic indices. In the dynamic VRP model, many scholars have designed both exact algorithms such as benders decomposition [24] and column generation [25] and other heuristic algorithms such as the improved particle swarm optimization algorithm [26] and taboo search [27,28] to solve the problem.

We formulate a vehicle path-planning model with a focus on explicitly deciphering the spatial and temporal distribution characteristics in the carbon dioxide emission trajectories associated with freight vehicles from micro-individual perspectives. Our model is based on the architecture of the CMEM. It also incorporates the freight vehicle travel time discretization technique and introduces the dynamic time-varying multi-path selection strategy compared with the static single-path policy [29]. The experimental results confirm the superiority of our model compared to other models [30,31]. This is a great innovation, because if logistics companies can obtain the details of the spatial and temporal characteristics of carbon dioxide emissions from micro-individual vehicles when planning vehicle paths compared with only the calculation of total freight vehicle carbon dioxide emissions [10,22,32], it will help the government and enterprises to make precision-driven strategies for carbon dioxide emission reduction.

In the remainder of this paper, we first describe the model and methods in Section 2. In Section 3, we analyze the results of the experiment. In Section 4, we discuss the nu-

merical results from different perspectives. Finally, we summarize our work and provide suggestions for future research in Section 5.

2. Model and Methods

The urban distribution network is mathematically described as a quintuple, denoted as $G = (V, A, P, V\prime, A\prime)$. Within this framework, V denotes the collection of customer nodes, A represents the ensemble of arcs connecting two different customer nodes, P denotes the set of paths connecting two customer nodes, $V\prime$ means the set of intersection nodes inherent in the road network, and $A\prime$ denotes the set of road segments within the road network. The arc connecting customer points i, j is $arc_{ij} \in A$. Here, p_{ij}^{p} denotes the freight vehicle's choice of path p in arc_{ij}, $p \in P$. In the urban road network, the distribution vehicle can choose more than one path between two customer nodes, and the travel speed and time of each path will change dynamically within different time periods [33,34]. Therefore, when planning vehicle distribution paths in the dynamic urban road network, it is necessary to consider the impact of vehicle travel speed and travel time with the congestion of different time periods on the road, and to choose the best paths between the customer nodes to minimize the total fuel consumption and carbon dioxide emissions of the freight vehicles.

2.1. Comprehensive Modal Emission Model (CMEM)

There are many vehicle exhaust emission models, such as Mobile Source Emission Model (MOBILE), EU Standard Vehicle Emissions Calculator (COPERT), EMission FACtor (EMFAC), Motor Vehicle Emission Simulator (MOVES), International Vehicle Emission (IVE), and so on. Among them, the CMEM has gained significant prominence due to its widespread application in various transportation research fields, such as microscopic traffic simulation [35], signal control simulation [36], and toll booth traffic operation analysis [37]. The model's architecture is based on three key modules: engine, speed, and load [22].

$$C = w \cdot fuel \tag{1}$$

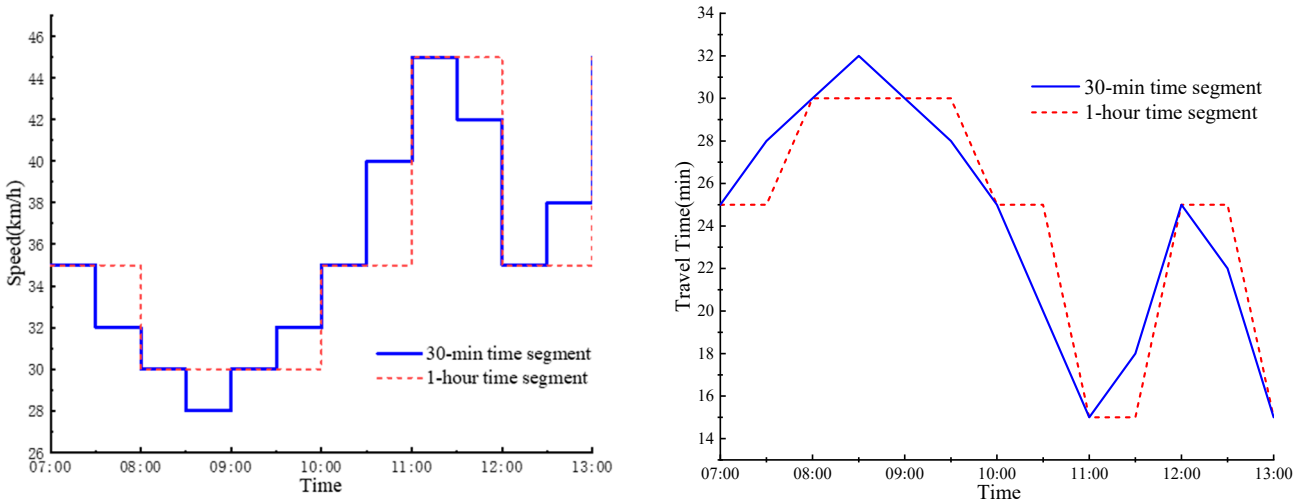
$$fuel(t, v, \mu, q, l) = \delta_1 t + \delta_2 v^3 t + \delta_3 (\mu + q) l \tag{2}$$

In the above equation, C is the total carbon dioxide emissions of the vehicle and the coefficient w is defined as the quantity of kilograms of CO_2 emitted per liter of fuel. Concurrently, $fuel$ is the fuel consumption of the freight vehicle, where δ_1, δ_2, and δ_3 represent the coefficients associated with the engine module, the speed module, and the vehicle load module, respectively. Furthermore, t, v, and l denote the travel time, speed, and distance travelled by the lorry, respectively. The parameters μ and q are the curb weight and load capacity of the freight vehicle.

2.2. Freight Vehicle Travel Time Discretization within Dynamic Time-Varying Road Networks

In the traditional paradigm of the vehicle path optimization problem, the travel time of a vehicle on a road segment is based on the linear distance between two customer points and a constant vehicle speed. Contrastingly, in the context of a dynamic, time-varying road network, the travel time of a freight vehicle on a road segment depends on the congestion level of each road segment, coupled with the average vehicle speed over different time intervals.

For analytical convenience, we divide the vehicle delivery time into N discrete time segments, each of which is one hour, 30 min, and so on. Within these segments, the vehicle speed on each road section is assumed to be constant. By considering the average speed of a road segment as a step function over time, as shown in Figure 1a, and the travel time as a linear segmented function of time, depicted in Figure 1b, we establish a coherent framework. In addition, when the time segment is divided into smaller ones (namely, 30 min), the travel time curve becomes smoother, as shown in Figure 1b. This refined granularity improves the temporal accuracy of the model and yields road network values that closely approximate actual traffic conditions.



(**a**) Travel speed (**b**) Travel time

Figure 1. Travel speed and time in different time segments.

When a delivery vehicle travels a consistent path over multiple time intervals, the evaluation requires a discrete assessment of the vehicle's travel speed and travel time within each individual time segment. This requires the aggregation of these calculated values across all time segments to obtain the final results. As illustrated in Figure 2, a truck's journey starts from Customer 1 and continues to Customer 2, traversing three road sections (a, b, and c) and negotiating two junctions. A notable scenario unfolds when road section b spans two different time periods, namely, 8:50–9:00 and 9:00–9:05. Consequently, the lorry's journey time on this particular road section has to be calculated separately for each time segment, and then the results are cumulated.

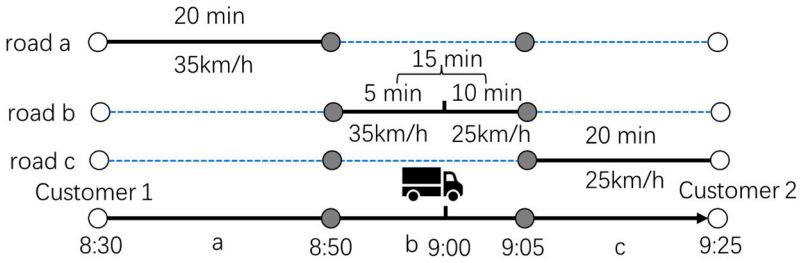


Figure 2. Travel time across different time segments.

2.3. Multi-Path Selection within Dynamic Time-Varying Road Network

Classical vehicle path problems typically assume that there is only a single route between two customer nodes [29], which is at odds with the complex realities of logistics and distribution operations. In the dynamic time-varying network considered in this study, a different perspective is adopted, positing the potential existence of multiple paths between two customers within an urban distribution network. The determinant for distribution vehicles to identify the optimal path is not the consideration of the shortest travel distance, but the least total travel time. We can use Algorithm 1 to find the optimal path between two customers *i*, *j*. In Algorithm 1, freight vehicles can choose between two path selection strategies, namely, static path scheme or dynamic path scheme.

Algorithm 1 Finding the optimal vehicle travel path in dynamic, time-varying road network.

Step 1: Initiate the segmentation of the freight vehicle delivery range into discrete N intervals defined in units of one hour, 30 min, etc.
Step 2: Update the current road condition data within the road network periodically at the beginning of each time segment. To access real-time traffic information, traffic status data covering the road network—including parameters such as congestion levels and average vehicle speeds—can be obtained through the Map API.
Step 3: Identify the time interval, denoted as k, corresponding to the departure moment of customer i. Subsequently, explore all feasible vehicle paths connecting customer nodes i and j within this time segment.
Step 4: Compute the travel times for all potential paths between customer points i and j. This calculation integrates the latest road condition and geographical distance data. Once computed, the paths are arranged in ascending order of travel time and stored within a designated path set. To reduce the computational and storage demands, if the number of searched paths is too large, only the first n best paths can be selected and stored in the path set.
Step 5: Evaluate the travel times associated with the paths within the path set. If these travel times are below a pre-determined time threshold—e.g., 10 min—proceed to Step 6 (Static Path Scheme). Alternatively, proceed to Step 7 (Dynamic Path Scheme).
Step 6: Static Path Scheme. Since the travel times of the paths within the path set are all within the specified time threshold, select the path with the shortest travel time. This path becomes the chosen trajectory for the freight vehicle to travel from customer node i to customer node j.
Step 7: Dynamic Path Scheme. If the travel times of the paths in the path set all exceed the specified time threshold, it is conceivable that the shortest time path selected by the delivery vehicle within time segment k, which was originally considered optimal, may evolve into a less favorable option over the course of the vehicle's journey due to changing conditions. As the temporal position of freight vehicle coincides with the start of time segment $k + 1$, the location of the vehicle, denoted as node h, is determined. The congestion information within the road network is then updated in accordance with the latest geographical and traffic data. Then, restart the path selection for the route between nodes h and j using the latest road network information, and return to Step 4.
Step 8: Stop the process when the freight vehicle completes its customer visits and returns to the distribution center.

2.4. Model Construction

2.4.1. Assumption and Notation

In order to simplify the vehicle path optimization problem, we introduce the following assumptions:

(1) Singular distribution center. There is only a single distribution center that serves as both the origin and destination for all distribution vehicles.
(2) Path diversity. Vehicles travelling from one customer node to another have the flexibility to choose multiple paths.
(3) Real-time path selection. Path selection is informed by the real-time average speed and travel time associated with each path within the road network.
(4) Unique customer service. Each customer is served exclusively by a single distribution vehicle, while a single vehicle can serve multiple customers.
(5) Service time exemption. Vehicles do not consume fuel during customer service.
(6) Variable load. The cumulative weight of the vehicle's cargo varies during the delivery course depending on the demand at the customer node being serviced.

In accordance with these assumptions, the model's notations are delineated as shown in Tables 1 and 2. The parameters included in the model are categorized into four different classes: network, vehicle, road, and physical parameters.

Table 1. Description of notations in model.

Notations	Interpretation	First Appeared in Section
Network		
V	Set of customer nodes, $V = \{0, 1, \cdots, n\}$, where 0 is the distribution center and $V \backslash \{0\}$ is the set of customer nodes	Section 2
A	Set of arcs connecting client nodes	Section 2
P	Set of paths connecting client nodes	Section 2
arc_{ij}	Arcs connecting client points i, j, where $i, j \in V \backslash \{0\}$ and $arc_{ij} \in A$	Section 2
p_{ij}^{p}	Choose path p in arc_{ij}, $p \in P$	Section 2
$V\prime$	Set of intersections in the road network	Section 2
$A\prime$	Set of road segments in the road network	Section 2
K	Number of delivery vehicles	Section 2.4.2
d_i	Demand of customer i	Section 2.4.2
s_i	Service time for client i	Section 2.4.2
a_i	Left time window of client i	Section 2.4.2
b_i	Right time window of client i	Section 2.4.2
E	Left time window of the distribution center	Section 2.4.2
L	Right time window of the distribution center	Section 2.4.2
l_{ij}^{p}	Distance of path p_{ij}^{p} connecting clients i, j	Section 2.4.2
τ_{ij}^{ph}	Travel time of the vehicle within time interval $[T_h, T_{h+1}]$ on path p_{ij}^{p}	Section 2.4.2
v_{ij}^{ph}	Average speed of the vehicle within time interval $[T_h, T_{h+1}]$ on path p_{ij}^{p}	Section 2.4.2
q_{ij}	Cargo volume of trucks on arc (i, j)	Section 2.4.2
q_{ij}^{p}	Cargo volume of trucks on path p_{ij}^{p}	Section 2.4.2
ω_{ij}^{ph}	Earliest departure time from customer i within time interval $[T_h, T_{h+1}]$ on path p_{ij}^{p}	Section 2.4.2
η_{ij}^{ph}	Waiting time in customer i within time interval $[T_h, T_{h+1}]$ on path p_{ij}^{p}	Section 2.4.2
w_{ij}^{ph}	Actual departure time from customer i within time interval $[T_h, T_{h+1}]$ on path p_{ij}^{p}	Section 2.4.2
x_{ij}	Equal to 1 if arc_{ij} is on the optimal route	Section 2.4.2
x_{ij}^{p}	Equal to 1 if the vehicle chooses the path p_{ij}^{p}	Section 2.4.2
x_{ij}^{ph}	Equal to 1 if the vehicle's departure time from customer i is within time interval $[T_h, T_{h+1}]$ on path p_{ij}^{p}	Section 2.4.2
δ_1	Engine module coefficient $\delta_1 = \frac{\zeta}{\kappa\psi} k N_0 V$	Section 2.1
δ_2	Speed module coefficient $\delta_2 = 0.5 \frac{\zeta}{\kappa\psi} \cdot \frac{1}{1000\varepsilon\omega} C_d A_f \rho$	Section 2.1
δ_3	Vehicle load module coefficient $\delta_3 = \frac{\zeta}{\kappa\psi} \cdot \frac{1}{1000\varepsilon\omega} [g \cdot \sin(\varphi) + g \cdot C_r \cdot \cos(\varphi)]$	Section 2.1

Table 2. Notations of CMEM.

Parameters	Interpretation	Initial Value
Vehicle		
ε	Vehicle transmission efficiency coefficient	0.4
k (kJ/rev/l)	Engine friction coefficient	0.2
N_0(rev/s)	Engine RPM	33.3
V(l)	Engine displacement	4.25
ω	Efficiency parameters of vehicle engines	0.9
A_f(m^2)	Vehicle windward area	5.2
Q (kg)	Maximum cargo capacity of distribution vehicles	200
μ (kg)	Curb-weight of distribution vehicles	2560

Table 2. *Cont.*

Parameters	Interpretation	Initial Value
Road		
φ	Angle of inclination of the road	0
C_r	Vehicle rolling resistance coefficient	0.01
Physical		
κ (kJ/g)	Typical fuel calorific value	44
ψ (g/L)	Fuel conversion factor	737
C_d	Atmospheric drag coefficient	0.7
ζ	Fuel-to-air mass ratio	1
ρ (kg/m^3)	Atmospheric density	1.205
g (m/s^2)	Gravitational constant	9.81

2.4.2. Mathematical Model

Based on the above description, we construct a mixed-integer planning model with the optimization objective of minimizing the carbon dioxide emissions of freight vehicles. This model takes into account the dynamic variation inherent in the road network.

$$\min C = w(fuel_1 + fuel_2 + fuel_3) \tag{3}$$

$$fuel_1 = \sum_{arc_{ij} \in A} \sum_{p \in P} \sum_{h \in [T_h, T_{h+1}]} \delta_1 \tau_{ij}^{ph} x_{ij}^{ph} \tag{4}$$

$$fuel_2 = \sum_{arc_{ij} \in A} \sum_{p \in P} \sum_{h \in [T_h, T_{h+1}]} \delta_2 \left(v_{ij}^{ph}\right)^3 \tau_{ij}^{ph} x_{ij}^{ph} \tag{5}$$

$$fuel_3 = \sum_{arc_{ij} \in A} \sum_{p \in P} \delta_3 (\mu + q_{ij}^p) l_{ij}^p x_{ij}^p \tag{6}$$

Equation (3) is the optimization objective of the model, which represents the minimum cumulative carbon dioxide emissions and fuel consumption of the distribution vehicle. The total vehicle fuel consumption of the vehicle is the result of the fuel consumption of the vehicle's engine, the speed at which the vehicle travels, and the load modules carried by the vehicle.

(1) Standard Constraints:

$$\sum_{j \in V \backslash \{0\}} X_{0j} \leq K \tag{7}$$

$$\sum_{j \in V \backslash \{0\}} X_{j0} \leq K \tag{8}$$

$$\sum_{i \in V} x_{ij} = 1, \forall j \in V \backslash \{0\} \tag{9}$$

$$\sum_{j \in V} x_{ij} = 1, \forall i \in V \backslash \{0\} \tag{10}$$

$$\sum_{i \in V} q_{ij} - \sum_{k \in V} q_{jk} = d_j, \forall j \in V \backslash \{0\} \tag{11}$$

Constraints (7) and (8) explicitly limit the number of delivery vehicles to a maximum of K units. Meanwhile, Constraints (9) and (10) rigorously establish the unambiguous principle that each customer must be served exactly once, thereby ensuring a unity degree of ingress

and egress for each customer node. Within this framework, Constraint (11) specifies the guarantee that each customer will be delivered a quantity equal to the difference between the load carried by the vehicle on arrival and on departure.

(2) Path Constraints:

$$\sum_{p \in P} x_{ij}^{p} = x_{ij}, \forall acr_{ij} \in A \tag{12}$$

$$\sum_{p \in P} q_{ij}^{p} = q_{ij}, \forall acr_{ij} \in A \tag{13}$$

$$d_j x_{ij}^{p} \leq q_{ij} \leq (Q - d_i) x_{ij}^{p} \tag{14}$$

Constraints (12) and (13) clarify that a vehicle traversing arc (i, j) is restricted to selecting a single trajectory for its passage. Concurrently, Constraint (14) meticulously ensures that the load capacity of each vehicle remains within the limits of the maximum cargo capacity as the vehicle traverses path p of arc (i, j).

(3) Time Constraints:

$$\sum_{h \in [T_h, T_{h+1}]} x_{ij}^{ph} = x_{ij}^{p}, \forall acr_{ij} \in A, p \in P \tag{15}$$

$$b_i x_{ij}^{ph} \leq w_{ij}^{ph} \leq b_{i+1} x_{ij}^{ph} \tag{16}$$

$$\omega_{ij}^{ph} + \eta_{ij}^{ph} = w_{ij}^{ph} \tag{17}$$

$$\omega_{0j}^{ph} = E x_{0j}^{ph} \tag{18}$$

$$\sum_{p \in P} \sum_{h \in [T_h, T_{h+1}]} (\tau_{i0}^{ph} x_{io}^{ph} + w_{i0}^{ph}) \leq L, \forall i \in V \backslash \{0\} \tag{19}$$

$$\sum_{i \in V} \sum_{p \in P} \sum_{h \in [T_h, T_{h+1}]} (w_{ij}^{ph} + \tau_{ij}^{ph} x_{ij}^{ph} + s_i) = \sum_{h \in V} \sum_{p \in P} \sum_{h \in [T_h, T_{h+1}]} \omega_{jh}^{ph}, \forall j \in V \backslash \{0\} \tag{20}$$

Constraint (15) denotes the time span within which the vehicle is located while traversing path p of arc (i, j). Constraint (16) indicates the temporal threshold that limits the departure of the vehicle from customer point i. Furthermore, Constraint (17) is the temporal continuity limit of the vehicle at customer i. Additionally, Constraints (18) and (19) indicate the temporal constraints that dictate both the departure and re-entry times for the vehicle at the distribution center. Finally, Constraint (20) is the time continuity limit of the vehicle along the arc (i, j).

(4) Other Constraints:

$$x_{ij}, x_{ij}^{p}, x_{ij}^{ph} \in \{0, 1\}, \forall arc_{ij} \in A, \forall p \in P, \forall h \in [T_h, T_{h+1}] \tag{21}$$

$$q_{ij}, q_{ij}^{p} \geq 0, \forall arc_{ij} \in A, \forall p \in P \tag{22}$$

$$w_{ij}^{ph}, \eta_{ij}^{ph}, \omega_{ij}^{ph} \geq 0, \forall arc_{ij} \in A, \forall p \in P, \forall h \in [T_h, T_{h+1}] \tag{23}$$

Constraint (21) embodies a binary constraint, while Constraints (22) and (23) manifest as variables subject to non-negativity constraints.

2.4.3. Algorithm Design

The genetic algorithm, conceived as a heuristic approach derived from the principles governing the natural evolution of organisms, has been widely applied to various engineering dilemmas. Its merits, which include scalability, robust convergence, and resilience, have underlined its effectiveness. Nevertheless, the genetic algorithm operates as a stochastic search technique. When juxtaposed with deterministic algorithmic paradigms, its utility in tackling large and complex optimization challenges may suffer from a pronounced reliance on initial solution quality, susceptibility to local optima trapping, and comparatively restrained convergence speed.

The intricacies of the dilemma considered in this study are beyond the scope of conventional VRP. Consequently, the conventional genetic algorithm requires refinement in order to accelerate the convergence rate and enhance its ability to uncover optimal solutions. In this model, the improvements we have made to the genetic algorithm are shown: firstly, a redesigned chromosome encoding methodology; secondly, the incorporation of binary tournament selection; and thirdly, the formulation of a localized search operation comprising two distinct components—namely, the destructive operation and the reparative operation.

(1) Coding Method

The effectiveness of the genetic algorithm in solving problems depends on the method used to encode the chromosomes—an aspect of paramount importance. A concise and understandable encoding approach has the potential to significantly increase the efficiency of problem solving. In this context, the natural number encoding technique is chosen. Since the number of customers is N and the upper limit for delivery vehicles is K, the chromosome length is $N + K - 1$. The schematic representation of the individual chromosome coding is visually illustrated in Figure 3.

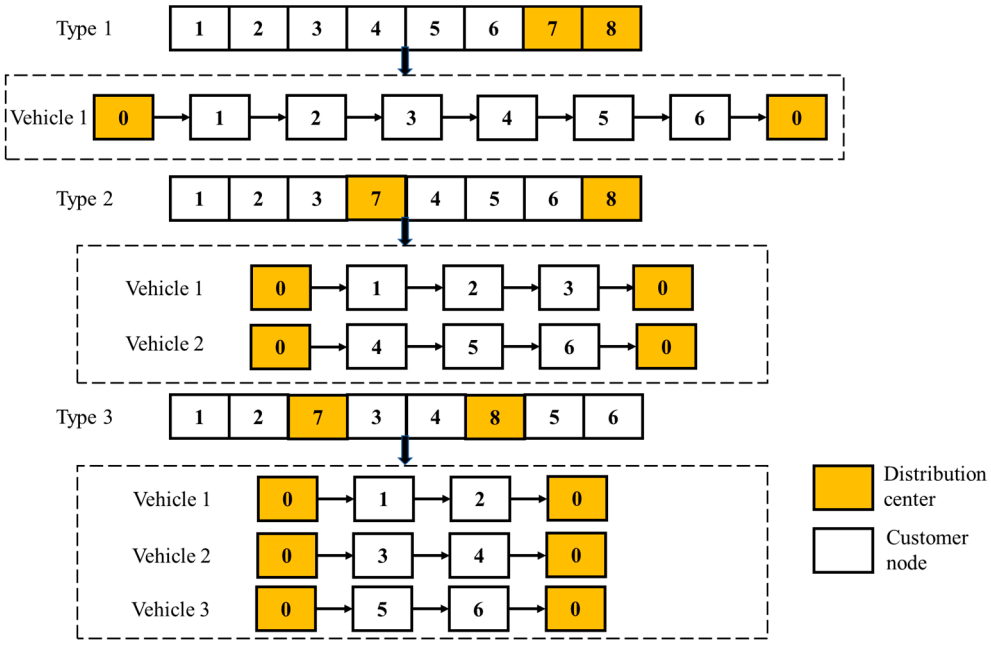


Figure 3. Chromosome coding scheme.

(2) Binary Tournament Selection Operation

The tournament method involves the process of extracting a defined number of chromosome individuals from the population at each iteration, and then determining the most fit candidate for integration into the next generation. Specifically, the binary tournament selection framework employed in this study involves a random head-to-head comparison between two chromosome individuals, culminating in the preference for the individual with the highest fitness score to be introduced into the forthcoming sub-population. Should

the population size be N, the selection procedure requires N iterations, with each round yielding a randomized pair of different individuals for evaluation, resulting in the selection of the superior performer. In cases where duplicates occur within the selected sub-population, only one of the duplicates is retained.

(3) Cross Operation

In the crossover operation, a pair of chromosomes is randomly selected as the parental units, as shown in Figure 4. Two crossover positions are then randomly chosen on these chromosomes, illustrated here as positions 3 and 6. The gene segment '3456' present on chromosome 1 is translocated to the beginning of chromosome 2. Concurrently, the gene segment '5432' from chromosome 2 is moved to the leading position of chromosome 1. The duplicated second gene within each chromosome is then sequentially excised from left to right, culminating in the final pair of offspring individuals.

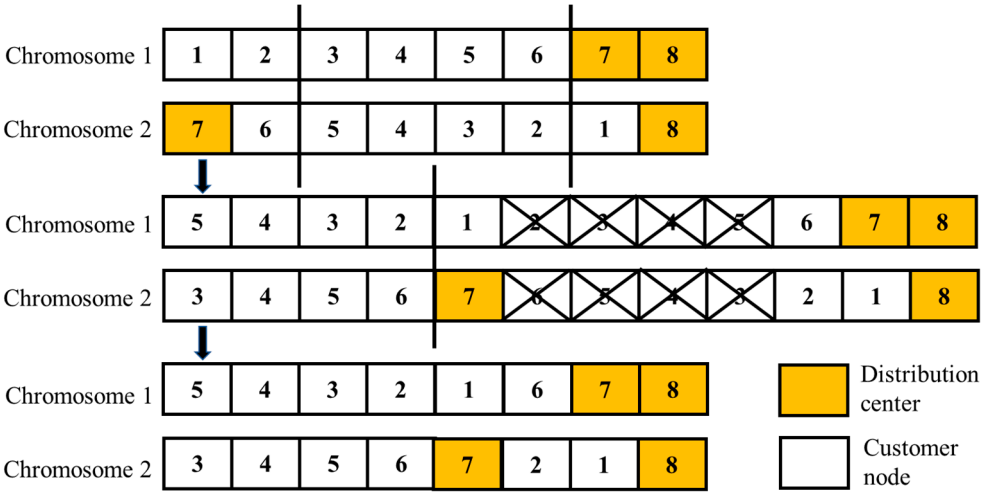


Figure 4. Chromosome cross operation.

(4) Mutation Operation

The probability of a mutation occurring during the evolution of a population is relatively small, so the mutation operation plays an auxiliary role. The mutation operation is relatively simple. Two mutation positions are randomly selected on a chromosome, and then the genes at these positions are swapped directly, as shown in Figure 5.

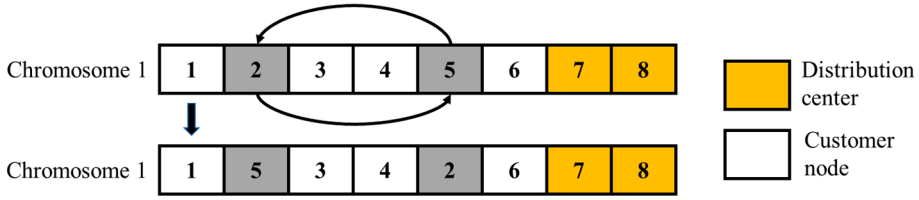


Figure 5. Chromosome mutation operation.

The probability of a mutation occurring in the course of population evolution remains comparatively low, making the mutation operation a minor facet. By its nature, the mutation process is relatively straightforward. Two mutation positions are randomly identified within a given chromosome and the genes at these positions are directly swapped.

(5) Local Search Operation

The local search operations are inspired by the concept of disruption and repair inherent in extensive domain search algorithms. This involves the initial application of a perturbation algorithm, which aims to selectively remove a subset of customers from the

dominant solution. This is followed by the repair operator, which reinserts the previously extracted customers into the perturbed solution. The interplay between these two facets is explained in Algorithms 2 and 3.

Algorithm 2 Destroying operation.

Input: current solution S, number of customers to be removed n
Output: solution after destruction S', set of removed customers I

1. Randomly select a customer v from S, $S' = S \backslash \{v\}$, $I = I \cup \{v\}$
2. While $|I| < n$
3. Randomly select customer v_i from set I
4. Calculate R(v_i,v_j), where j belongs to S and j does not belong to I
5. R(v_i,v_j) = $1/(c_{ij} + V_{ij})$, $c_{ij} = C_{ij}/\max(C_{ij})$.$V_{ij} = 0$, if v_i and v_j are served by the same vehicle; otherwise, $V_{ij} = 1$. C_{ij} is the fuel cost between i and j.
6. R_sort = sort (R, "descend")
7. v = R_sort(0), $S' = S' \backslash \{v\}$, $I = I \cup \{v\}$
8. End while
9. Return S' and I

Algorithm 3 Repairing operation.

Input: solution after destruction S', set of removed customers I
Output: repaired solution S

1. $S = S'$
2. While $|I| > 0$
3. Calculate the minimum insertion cost C_v for customer v, the insertion path number i with the minimum fuel cost, and the position pos on path i.
4. $C_v = C_1 - C_2$. C_2 and C_1 are the total costs before and after customer v is inserted into position pos of path i
5. v_m = argmax(C_v)
6. Insert customer v_m into path i at position pos
7. $I = I \backslash \{v\}$ and $S = S \cup \{v\}$
8. End while
9. Return S

3. Numerical Experiment and Results

3.1. Experimental Setup and Computational Environment

We offer an illustrative case of the vehicle-routing problem within a dynamic time-varying network with a single distribution center and ten different customers. The information of the distribution center and customers in networks is given in Table 3. We choose the urban road network from Changsha city of China, which is characterized by morning and evening peaks on weekdays, with road congestion fluctuating in synchrony with the time course of the day. Detailed description of the speeds of each road in the road network is in Appendix A.

The distribution center offers its services between 7:00 and 19:00, according to a 30 min time segmentation. The configuration of the distribution road network includes main arterials, secondary roads, and by-pass roads, as illustrated in Figure 6. Different road classifications result in different vehicle speeds and functional attributes. The main arteries play a critical traffic role within the urban network and are characterized by wide carriageways, more lanes, and higher vehicle speeds. By contrast, secondary roads have fewer and narrower lanes than their arterial counterparts. By-pass roads have the lowest number of lanes and the slowest speeds, and the cross-section of by-pass roads consists of only one single lane in each direction.

Table 3. The information of distribution center and customers.

No.	X Co-Ordinate	Y Co-Ordinate	Demand/kg	Left Time Window	Right Time Window	Service Time/min
0	0	28	0	0	720	0
1	0	24	40	20	60	20
2	6	24	10	60	150	10
3	6	20	20	90	150	15
4	12	20	16	160	200	15
5	0	16	40	180	270	25
6	12	16	30	300	360	15
7	9	12	10	390	440	10
8	6	8	15	430	490	10
9	3	4	20	480	570	15
10	9	0	15	600	670	10

Note: (1) No. 0 is the distribution center and 1–10 represent the customers; (2) In the time window, 0 represents the start service time and 720 represents the end service time of distribution center.

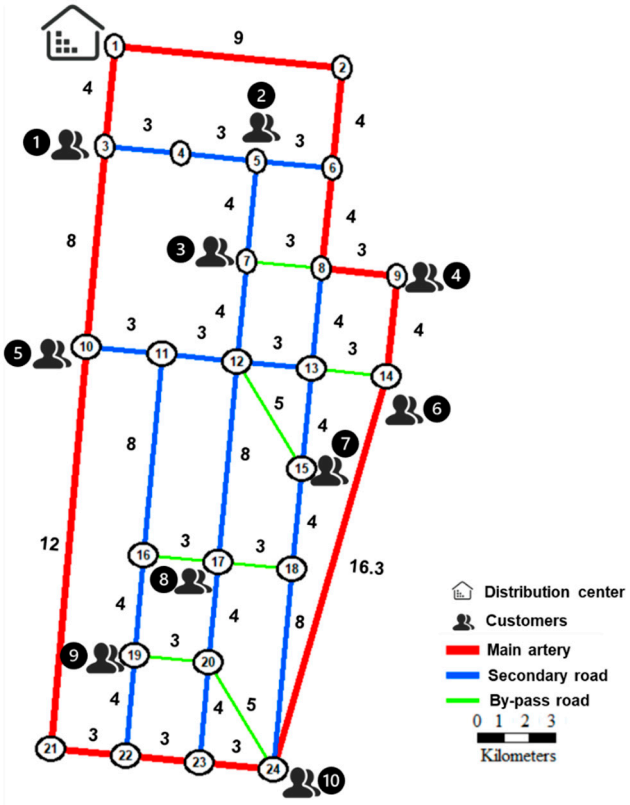


Figure 6. Road network for freight distribution.

We used MATLAB 2021a to tackle the problem, harnessing the computing power of a 12th generation Intel Core i9-12900K processor clocked at 3.20 GHz, paired with 64 GB of RAM, all running in the Windows 11 environment. To quantify vehicle fuel consumption, we used the CMEM, which allowed us to determine fuel consumption with a high degree of accuracy. The relevant parameters of the distribution vehicle are determined with reference to the light freight vehicle. The vehicle emission standard used is the National V standard and the diesel is 0#. The initial values for all parameters are detailed in Table 2.

3.2. Analysis of Experimental Results

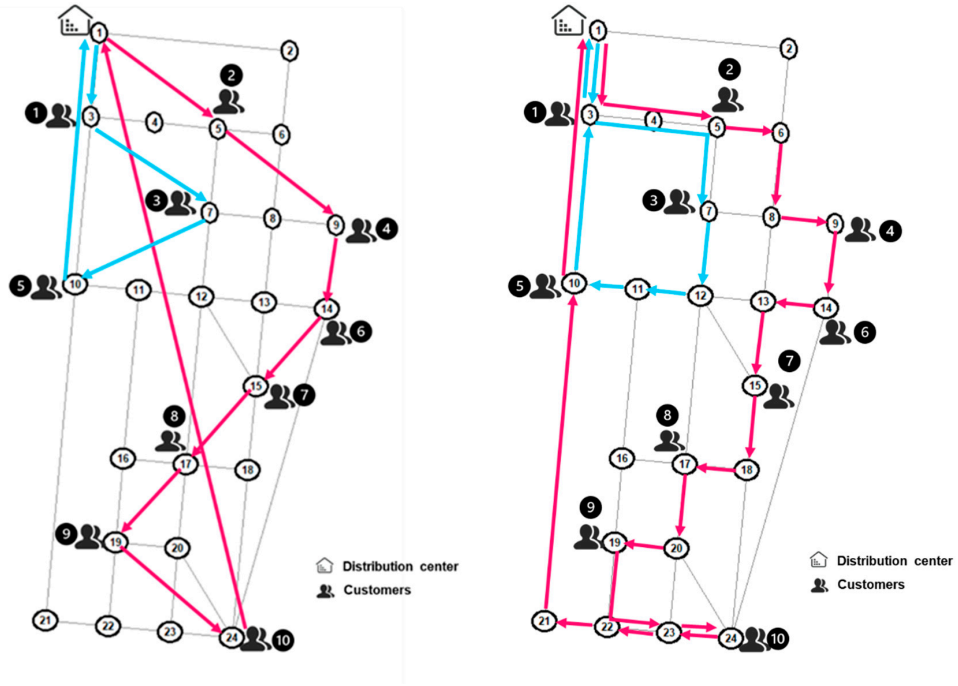
In the genetic algorithm, the population size is set to 100 individuals. The crossover probability and variance probability parameters are fine-tuned to 0.9 and 0.05, respectively. Moreover, the emission factor (measured in kilograms of CO_2 emitted per liter of fuel) is set to 2.63. The optimization process unfolded over a span of 250 iterative calculations, culminating in the achievement of the optimal vehicle delivery route. The detailed results of the experiment are shown in Table 4 (Model 1). The optimized distribution plan includes two distribution routes, the first being '0-2-4-6-7-8-9-10-0' and the second route being '0-3-5-1-0'.

Table 4. Details of the model results.

Model	Number of Vehicles	Distance (km)	Travel Time (min)	Fuel (Liter)	CO_2 Emitted (kg/d)	Description
1	**2**	**128**	**252.686**	**25.085**	**65.974**	**Our baseline model**
2	3	142	272.228	27.834	73.203	Consider 3 vehicles
3	2	128	246.914	26.289	69.140	Minimum travel time as objective function
4	2	142	273.428	28.562	75.118	Shortest Euclidean distance as objective function
5	2	128	248.657	25.071	65.937	1 h time segment
6	2	128	252.234	25.084	65.971	15 min time segment
7	2	128	249.458	25.068	65.929	Mixed time segment
8	2	128	259.771	26.301	69.171	Single-path selection
9	2	128	202.593	24.988	65.718	Weekend
10	2	134	271.577	26.407	69.450	The day before holiday

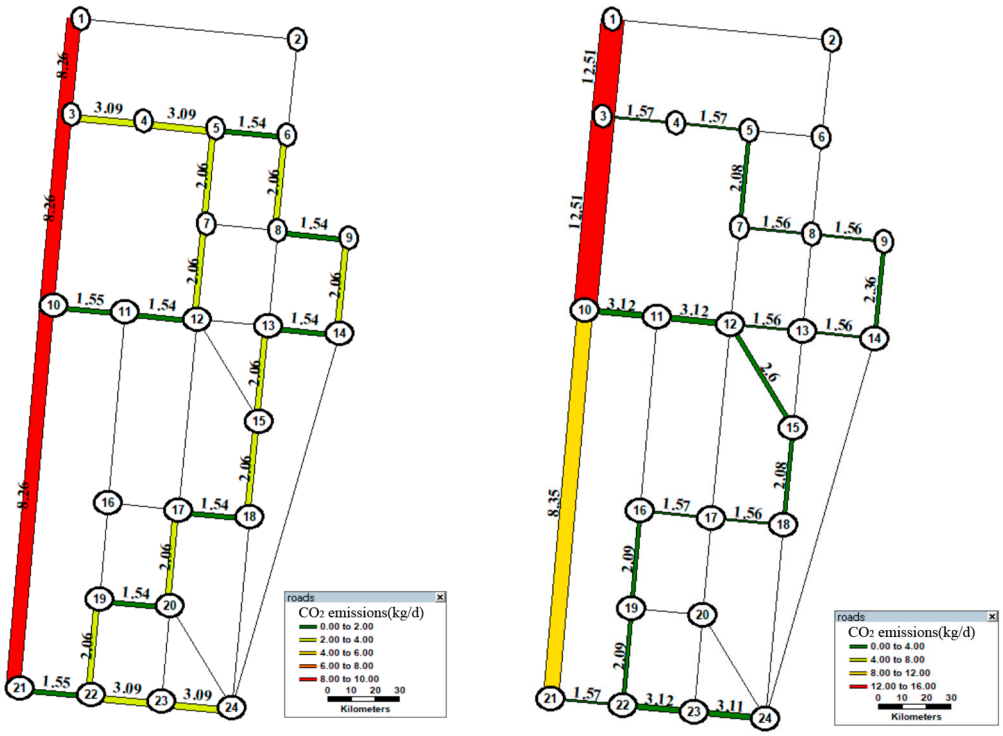
The visual representations encapsulated in Figure 7 include a dual perspective, consisting of a customer graph and a road network graph. Within the customer graph, the nodes symbolize customer points and the distribution center, while the arcs represent virtual routes connecting each customer. Conversely, in the road network graph, the nodes represent city intersections, and the arcs represent road segments that connect these intersections. It is noteworthy that an arc in the customer graph represents an amalgamation of multiple paths between two customers at different departure times as represented in the network graph.

In Figure 8a, we present the results detailing the spatial distribution of carbon dioxide emissions from the delivery vehicles within the road network. Given that the delivery vehicles take the form of light trucks, classified as unlimited trucks with blue license plates, they are allowed to travel in the city center during the day on weekdays. The figure shows that the road sections with higher carbon dioxide emissions are mainly concentrated around the customers. Carbon dioxide emissions are highest near the distribution center, mainly due to the close clustering of customers 1, 2, 3, and 5 near the distribution center. Road sections (1–3) and (3–10) also show high carbon dioxide emissions. Although these sections are urban trunk roads, the overlap of the vehicle delivery times with the morning and evening peak hours on urban roads, combined with high volumes of traffic on the lanes, results in a higher carbon dioxide emission intensity due to the lower average speed on these trunk roads.



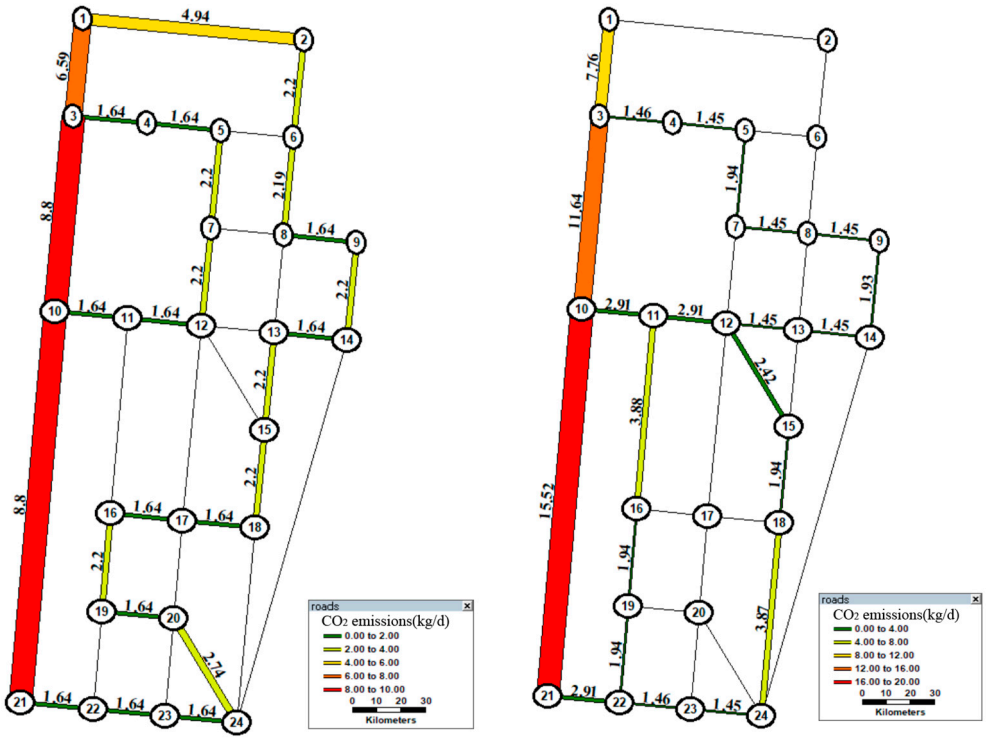
(**a**) Customer delivery routes (**b**) Vehicle distribution routes

Figure 7. Distribution route results.



(**a**) Model 1 (our baseline model) (**b**) Model 2

Figure 8. *Cont.*



(**c**) Model 3 (**d**) Model 4

Figure 8. Spatial distribution of carbon dioxide emissions on road networks.

The temporal distribution of carbon dioxide emissions over the road network, as shown in Figure 9 (Model 1), shows that the majority of carbon dioxide emissions are concentrated in the morning peak hours from 7:00 to 10:00. This distribution trend is due to the fact that Distribution Route 2 mainly services customers close to the distribution center, allowing for quicker task completion and enabling vehicles to complete their distribution tasks before noon.

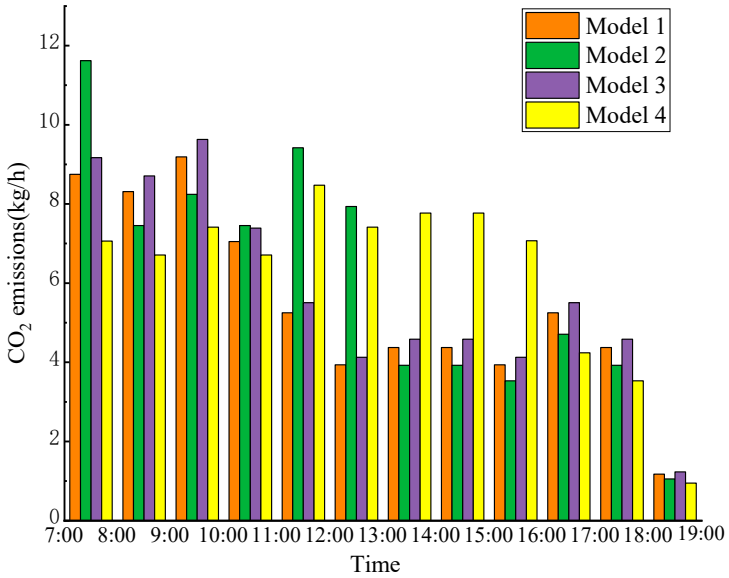


Figure 9. Temporal distribution of carbon dioxide emissions on road networks.

The cumulative analysis confirms the assertion that different customer requirements for distribution services lead logistics companies to choose different vehicle distribution

route strategies. These choices, in turn, have a marked influence on both the spatial and temporal patterns of carbon dioxide emissions from vehicles within the urban road network.

4. Sensitivity Analysis and Discussion

4.1. Assessment of Diverse Objective Function Models

Model 1 serves as our baseline model, and the experimental results show the selection of 2 vehicles, resulting in a total fuel consumption of 25.085 L and CO_2 emissions of 65.974 kg, as meticulously tabulated in Table 4. In Model 2, the number of transport vehicles is 3, while the other model parameters and constraints remain unchanged. Obviously, compared to Model 1, Model 2 gives a noticeable increase in total distance travelled of 10.94%, accompanied by an increase in travel time of 7.73% and an increase in CO_2 emissions of 10.96%.

Figure 8b illustrates a noticeable increase in carbon dioxide emission intensity within the main arterial paths close to the distribution center when more freight vehicles are included in Model 2. The temporal distribution, shown in Figure 9, further illustrated this increase, with pronounced increases in carbon dioxide emissions between 7 a.m. and 8 a.m. during the morning peak and between 11 a.m. to 13 p.m. at midday.

In Model 3, the optimization objective focused on reducing the total travel time of the transport vehicles [30]. Compared to the baseline, Model 3 decreases the travel time by 2.28%, albeit coupled with a 4.8% increase in CO_2 emissions. Notably, the carbon dioxide emissions in Model 3 tend to be more concentrated on main roads, exemplified by road sections such as (1–2), (2–6), etc. The objective of Model 3 is to prioritize the minimization of travel time for freight vehicles, which leads drivers to choose urban trunk roads characterized by a higher road class. The temporal distribution of carbon dioxide emissions within Model 3 mirrors that of Model 1, but with a higher emission per unit of time.

Model 4 is formulated with the aim of minimizing the total Euclidean distance travelled by freight vehicles [31]. A comprehensive examination of Table 4 underscores that Model 4 leads to a noticeable increase of 10.94% in the actual distance travelled by its vehicles, accompanied by a simultaneous increase of 13.86% in carbon dioxide emissions compared to the baseline model. Spatially, the distribution of carbon dioxide emissions within Model 4 reaches its zenith, particularly concentrating along primary roads, exemplified by segments like (10–21) and (3–10). Temporally, the distribution of carbon dioxide emissions in Model 4 is more evenly spread, even during off-peak hours such as (11:00–15:00), where the intensity of carbon dioxide emissions still remains significantly higher than in the other models.

Table 5 describes the distribution of carbon dioxide emissions from different types of roads, and the share of carbon dioxide emissions from Model 1 is 57.86%, 32.01%, and 10.13% for the main arteries, secondary roads, and by-pass roads, respectively. The carbon emission intensity of trunk roads is the highest, followed by secondary roads, and by-pass roads have the lowest carbon emission. Compared to Models 2, 3, and 4, the relatively low carbon dioxide emissions of main roads in Model 1 are due to the fact that the objective function of the other models is more homogeneous and direct, with an emphasis on the minimum travel time or the shortest Euclidean distance, and the travel paths tend to select main roads that carry a larger amount of traffic flow between the two customer points. The travel path selection in Model 1 is more flexible, not only selecting trunk roads, but also dynamically selecting between trunk roads and other types of roads, as the traffic flows on each road section in the network change at each moment.

Table 5. Carbon dioxide emissions in different types of roads (kg/d).

Model	Main Artery	Secondary Road	By-pass Road	Total
1	**38.17 (57.86%)**	**21.12 (32.01%)**	**6.68 (10.13%)**	**65.97**
2	45.08 (61.58%)	19.28 (26.34%)	8.84 (12.08%)	73.20
3	42.28 (61.15%)	17.55 (25.38%)	9.31 (13.47%)	69.14
4	44.12 (58.73%)	25.68 (34.19%)	5.32 (7.08%)	75.12
8	37.32 (53.96%)	18.12 (26.19%)	13.73 (19.85%)	69.17
9	35.28 (53.84%)	21.45 (32.63%)	8.89 (13.53%)	65.72
10	34.73 (50.01%)	20.84 (30.00%)	13.88 (19.99%)	69.45

4.2. Assessment of Varied Time Interval Segmentation

To assess the influence of different time segmentations on the model, we compare the results with Model 1 (30 min segmentation). This involves considering a 1 h segmentation (Model 5), a 15 min segmentation (Model 6), and a hybrid time segmentation (Model 7). The hybrid time segmentation is conceptually defined as follows: time intervals that span the transition phase between morning (or evening) peak and off-peak are assigned 15 min, while the remaining time intervals remain at 30 min, as visually presented in Figure 10.

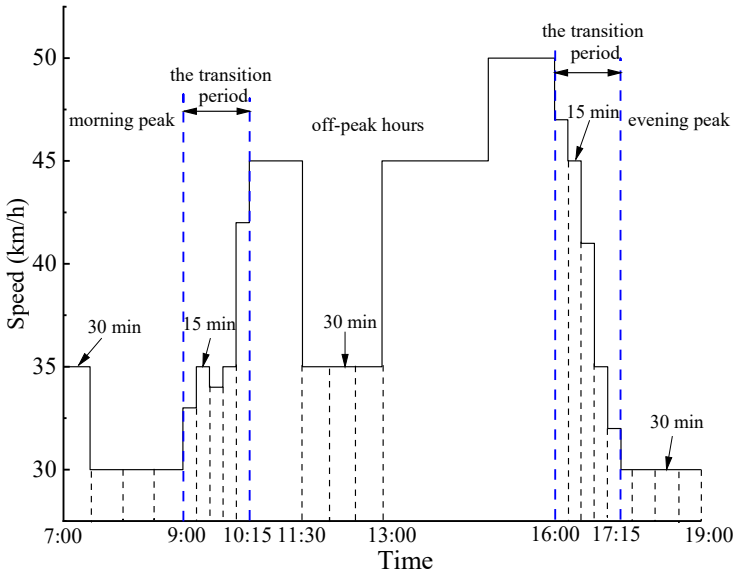


Figure 10. The mixed time segmentation (Model 7).

Derived from the data in Table 4, the results of Models 5, 6, and 7 show a relatively small deviation from the baseline model. In particular, the degree of precision in time segmentation is inversely correlated with the size of the time interval. In essence, smaller time intervals provide greater accuracy in the calculation of freight vehicle fuel consumption, and thus provide results that more closely reflect real-world road transport scenarios. This is consistent with the findings of reference [22]. However, in the context of a large urban road network comprising a significant number of roads (5000 or 10,000), the use of smaller time intervals leads to an increased data-processing workload and requires greater storage capacity. The use of mixed time intervals is a reasonable compromise. It ensures computational accuracy while minimizing the amount of data storage required.

4.3. Evaluation of Multi-Path Selection between Two Customers

The classical model postulates the selection of only a single optimal path between any two customers [29], yielding experimental results as shown in Table 4 (Model 8). Despite an analogous total travel distance, Model 8 leads to a 2.81% increase in vehicle travel time and a corresponding 4.79% increase in the total CO_2 emissions compared to the baseline model. This observation underscores that, when delivery vehicles are given the opportunity to

choose between different routes, they can make significant savings in terms of both delivery time [38] and carbon dioxide emissions. This benefit is largely attributed to the freedom that delivery vehicles have to choose alternative routes that are relatively free of congestion, based on real-time road conditions.

Logistics companies typically choose the shortest route between two customers when planning vehicle routes. However, given the dynamic changes in traffic flow and average speeds on the urban road network over time, the initially preferred route may no longer be optimal. This could result in longer delivery times, increased vehicle fuel consumption, and higher carbon dioxide emissions. If vehicles were able to consider multiple routes between two customers, their journeys could become more adaptive. In this way, vehicles might be inclined to choose alternative routes characterized by longer distances but faster average speeds. This strategic shift could effectively avoid traffic congestion, thereby reducing delivery times and minimizing carbon dioxide emissions.

4.4. Analysis of the Impact of Weekends and Public Holidays

In order to measure the different impacts of weekdays, weekends, and holidays on the carbon emission trajectories of freight vehicles, we compare Models 1, 9, and 10. Model 1 is tailored to weekdays, covering Monday to Friday. In contrast, Model 9 includes weekends, specifically Saturdays or Sundays. Model 10 focused on specific dates, namely, 30 April or 30 September—corresponding to the day before International Labor Day or the Chinese National Day. Examining the experimental results in Tables 4 and 5, it can be seen that Model 9 has lower total travel times and lower carbon dioxide emissions for the transport vehicles compared to Model 1. However, Model 10 bears the impact of holiday-related tourism and vacationing, resulting in significantly increased total travel distances, travel times, and carbon dioxide emissions for the transport vehicles.

Figure 11 provides a comprehensive representation of the average vehicle speeds on the main arteries of the urban road network in Models 1, 9, and 10. In Model 1, there is a striking pattern of time-varying dynamics characterized by the morning and evening peaks. Specifically, between 7:00 and 9:00 and 17:00 to 19:00, the traffic density on the main roads records a significant increase, which leads to a significant decrease in average speeds during these periods. Model 9, attributed to weekends, shows a reduced prominence of the morning and evening peaks. In this scenario, the average speed on the main roads remains relatively high and constant. Conversely, the dynamics of Model 10 are influenced by holidays, resulting in relatively lower speeds on main roads. Particularly, between 17:00 and 19:00, a strong influx of residents leaving their workplaces for leisure and travel causes significant congestion on the city's main arteries.

Figure 12 illustrates the temporal distribution patterns that characterize carbon dioxide emissions from transport vehicles. Model 9 is similar to Model 1. However, Model 9 benefits from increased average lane speeds, which allow transport vehicles to complete their freight distribution journey earlier. This, in turn, reduces carbon dioxide emissions during the evening peak. Conversely, Model 10 is heavily influenced by holiday-related dynamics, resulting in an accelerated proliferation of vehicles on the main roads and a corresponding increase in carbon dioxide emissions from freight vehicles. This escalation is particularly pronounced during the midday and evening peak periods.

In terms of the spatial distribution characteristics of carbon dioxide emissions from transport vehicles, as illustrated in Figure 13, Model 9 shows a carbon emission distribution similar to Model 1, albeit characterized by a relatively lower carbon emission intensity per unit distance. Model 10 differs significantly from Model 1 due to the increased volume of traffic on main roads during evening peak hours. This phenomenon leads to a strategic shift in route selection for returning delivery vehicles, favoring secondary roads such as '22-19-16-11-10' over the main road route '22-21-10'. The results thus demonstrate the ability of our multi-path benchmark model to detect and quantify the influence of holiday- related effects on the spatial distribution of carbon emission trajectories of transport vehicles, in contrast to conventional single-path models.

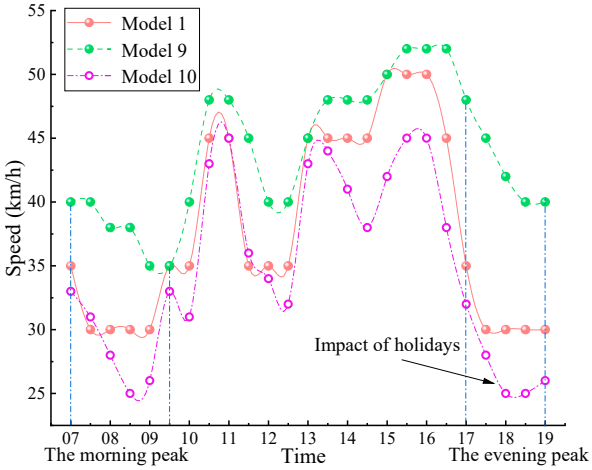


Figure 11. Speed changes on the main artery due to weekends and holidays.

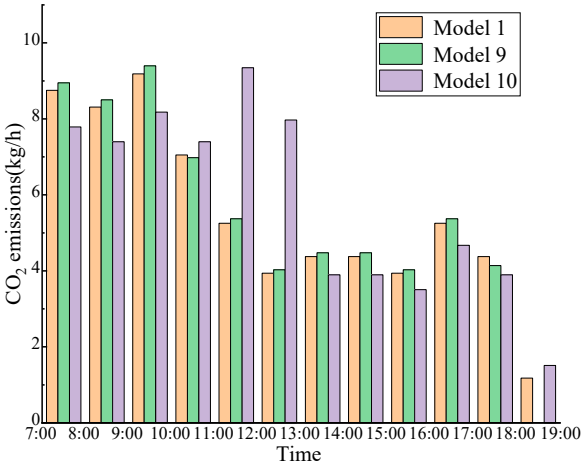
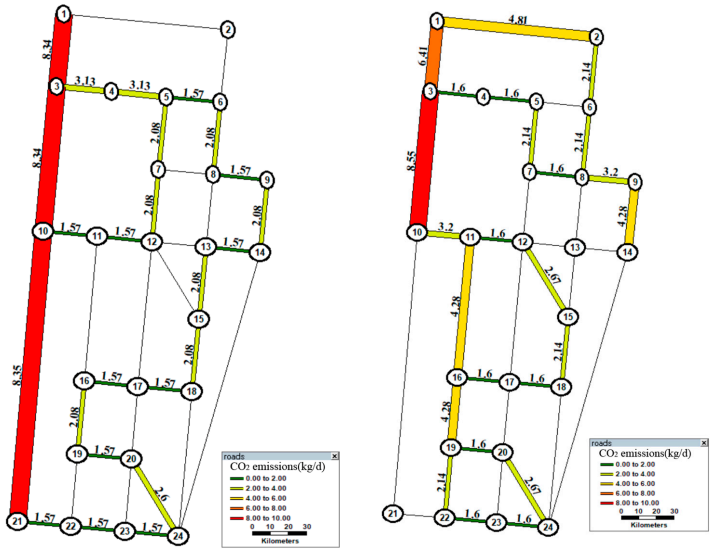


Figure 12. Temporal distribution of carbon dioxide emissions influenced by weekends and holidays.



(**a**) Model 9 (**b**) Model 10

Figure 13. Spatial distribution of carbon dioxide emissions influenced by weekends and holidays.

5. Conclusions

In the context of escalating concerns about global warming, the need to reduce the environmental impact of vehicle carbon dioxide emissions has become increasingly urgent. In the freight transport sector, the widespread adoption of new energy technologies remains limited, reinforcing the importance of investigating the characteristics of the carbon emission trajectories of freight vehicles. This research is of paramount importance to both governments and logistics companies in their pursuit of carbon reduction initiatives. This study formulates a vehicle path-planning model in the context of dynamic time-varying networks, which aims to capture the spatial and temporal distribution characteristics inherent in the carbon emission trajectories of freight vehicles. Central to this model is the minimization of total carbon dioxide emissions from vehicle distribution, based on the CMEM. To increase accuracy, the model employs the freight vehicle travel time discretization technique and introduces the dynamic time-varying multi-path selection strategy. The culmination of these efforts is the design of an improved genetic algorithm to solve this complex problem. Empirical results vividly illustrate the superior performance of our model over alternative objective function models. This is manifested in the reduction of total travel distance, travel time, and carbon dioxide emissions for the transport vehicles. In addition, our observations underscore the central role of accurate time segmentation within the scope of time segmentation considerations, delineating its profound influence on both vehicle carbon dioxide emissions and algorithmic efficiency. Finally, the experimental results underline that our multi-path model is able to detect the imprint of holiday-related effects on the spatial and temporal distribution of carbon emission trajectories, especially when compared to traditional single-path models. That is, within the multi-path network, delivery vehicles have the leeway to dynamically select different routes based on real-time road congestion, thereby compellingly reducing vehicle travel time and carbon dioxide emissions.

Although our benchmark model performs well on the given test instances, there are some limitations. Firstly, the road network we have chosen is relatively small, and future work should include larger road networks and a wider range of customers as instances. Secondly, our model assumes a single distribution center, which differs from the reality of logistics companies that maintain multiple distribution centers. Thirdly, we used a modified genetic algorithm to solve the model, but other optimization algorithms such as ant colony and simulated annealing may be considered in the future [39]. Finally, we will consider other variables such as driver behavior that also affects the fuel consumption and CO_2 emissions of freight vehicles, as well as other sustainable technologies to reduce carbon emissions in the freight sector in future studies.

Author Contributions: Methodology, R.S. and X.X.; formal analysis, R.S.; investigation, W.Q. and W.S.; resources, W.Q. and W.S.; data curation, X.X.; writing—original draft, R.S.; supervision, R.S. All authors have read and agreed to the published version of the manuscript.

Funding: This work was supported by the Ministry of Education of Humanities and Social Science Project "Research on parking demand forecast and parking space optimization allocation in urban residential areas" (20YJCZH133); the Social Sciences Funding Project of Hunan province "Research on parking demand prediction and parking space optimization allocation in urban residential areas based on sharing concept" (20YBQ113); the Natural Sciences Funding Project of Hunan province "Research on shared parking management in urban central area based on data sharing mode" (2022JJ40881); the Excellent Youth Project of the Hunan Provincial Department of Education "Research on urban freight demand forecast based on spatiotemporal big data" (21B0257); and the Science and Technology Project of Changsha city "Solution and technical implementation of shared parking timeout parking conflict" (kq2004092).

Institutional Review Board Statement: Not applicable.

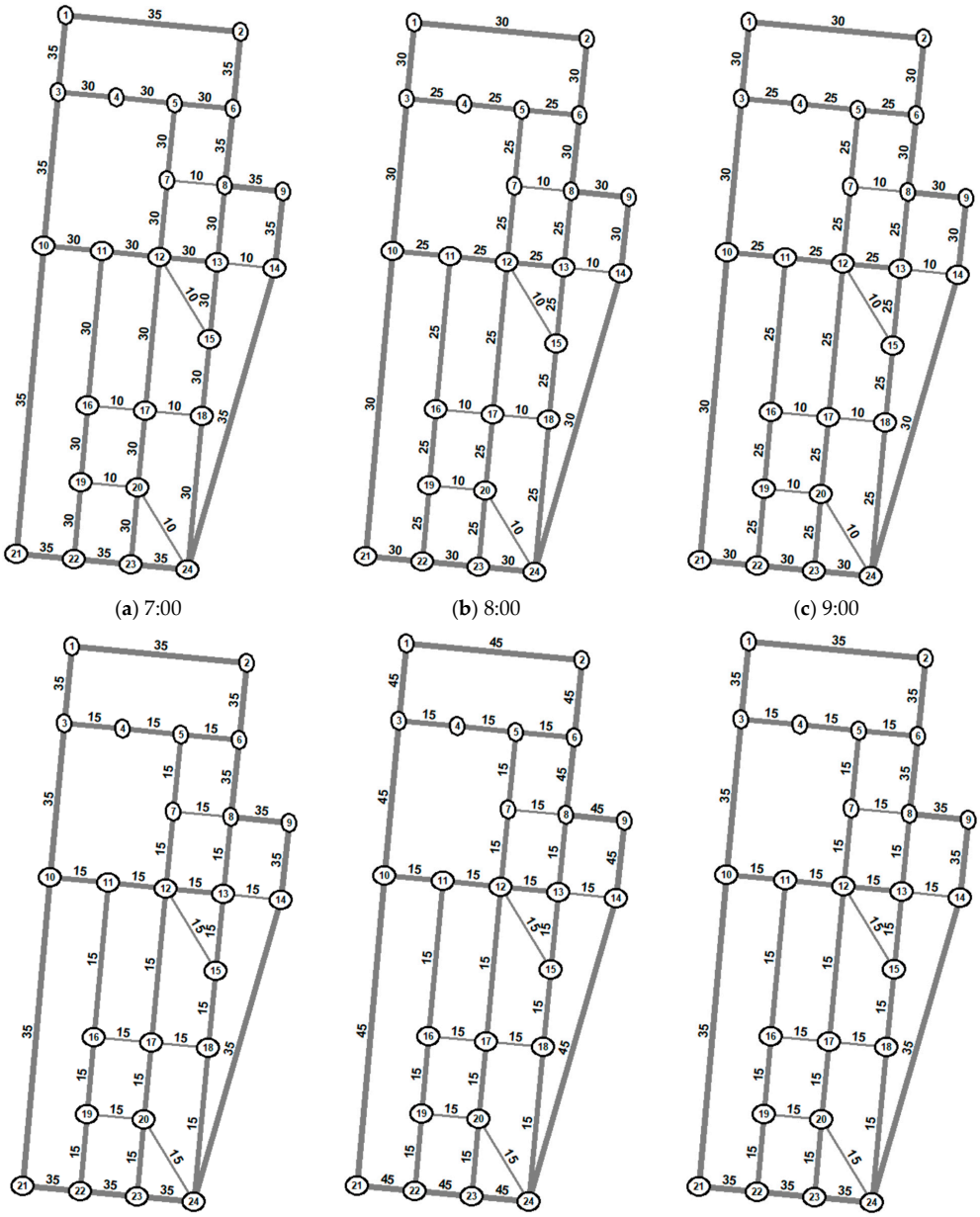
Informed Consent Statement: Not applicable.

Data Availability Statement: The original datasets used in the study are included in the article. Further inquiries can be directed to the corresponding author.

Conflicts of Interest: The authors declare no conflict of interest.

Appendix A. Traffic Speed

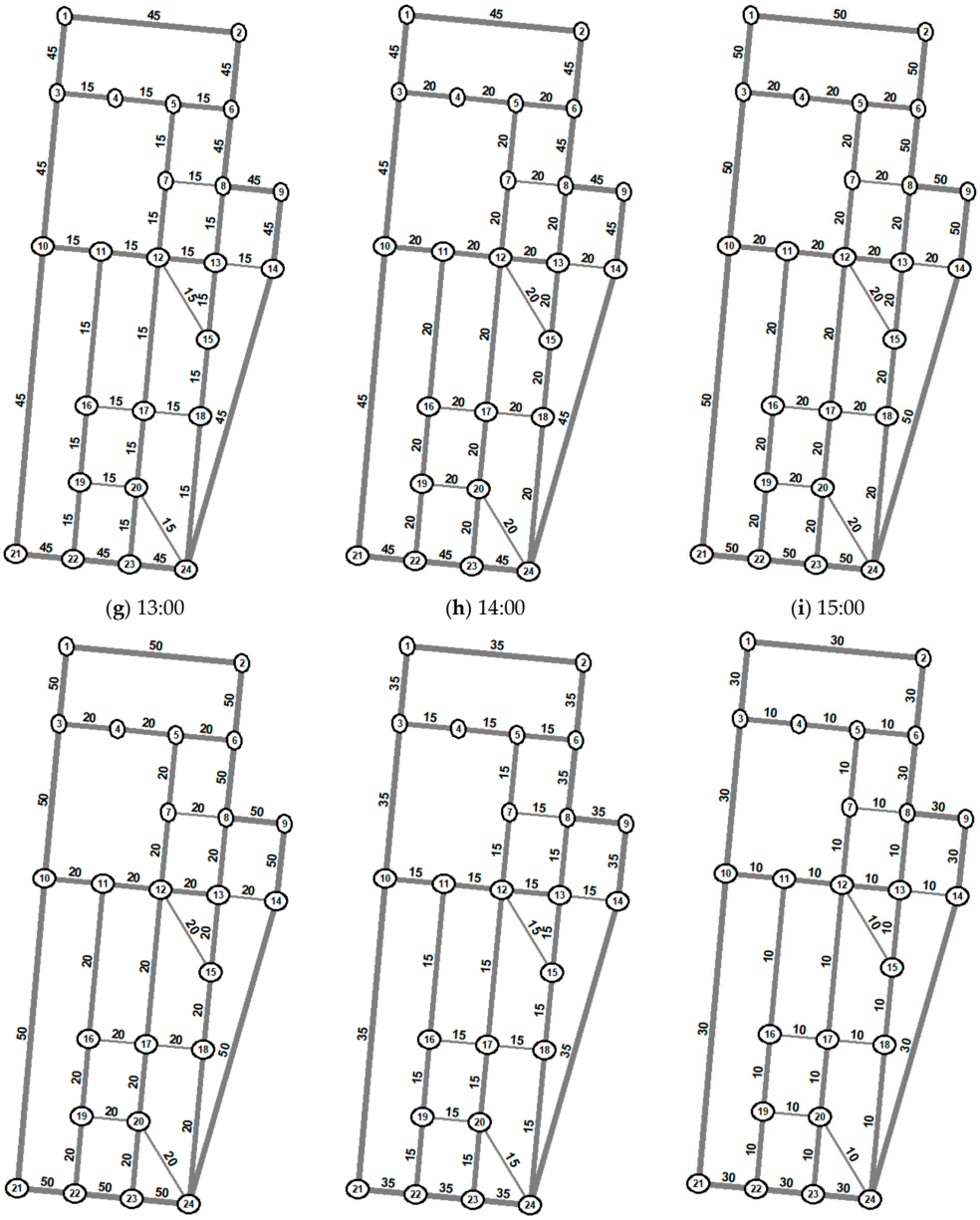
The speeds of each road in the road network are mainly collected from the Baidu Maps Traffic and Travelling Big Data Platform (https://jiaotong.baidu.com/congestion/city/urbanrealtime accessed on 17 September 2023), and partly from Figure A1, the field survey, due to the inaccessibility of some data. The average speeds in the road networks are collected in Changsha city of China from 7:00 to 19:00 on weekdays, as shown in Figure A1.



(**a**) 7:00 (**b**) 8:00 (**c**) 9:00

(**d**) 10:00 (**e**) 11:00 (**f**) 12:00

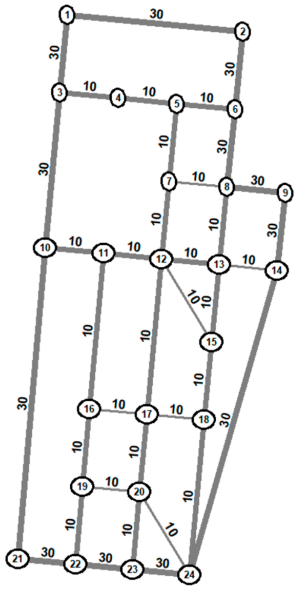
Figure A1. *Cont.*



(**g**) 13:00 (**h**) 14:00 (**i**) 15:00

(**j**) 16:00 (**k**) 17:00 (**l**) 18:00

Figure A1. *Cont.*



(**m**) 19:00

Figure A1. Speed (km/h) of the road network from 7:00 to 19:00 on weekdays.

References

1. Mao, H.; Shi, J.; Zhou, Y.; Zhang, G. The electric vehicle routing problem with time windows and multiple recharging options. *IEEE Access* **2020**, *8*, 114864–114875. [CrossRef]
2. Martinelli, R.; Contardo, C. Exact and heuristic algorithms for capacitated vehicle routing problems with quadratic costs structure. *INFORMS J. Comput.* **2015**, *27*, 658–676. [CrossRef]
3. Tencent Net. Available online: https://new.qq.com/rain/a/20220504A08IZY00 (accessed on 4 May 2022).
4. Ostermeier, M.; Henke, T.; Huebner, A.; Waescher, G. Multi-compartment vehicle routing problems: State-of-the-art, modeling framework and future directions. *Eur. J. Oper. Res.* **2021**, *292*, 799–817. [CrossRef]
5. Pasha, J.; Dulebenets, M.A.; Kavoosi, M.; Abioye, O.F.; Wang, H.; Guo, W. An optimization model and solution algorithms for the vehicle routing problem with a "factory-in-a-box". *IEEE Access* **2020**, *8*, 134743–134763. [CrossRef]
6. Young, G.O. Synthetic structure of industrial plastics. In *Plastics*, 2nd ed.; Peters, J., Ed.; McGraw-Hill: New York, NY, USA, 1964; pp. 15–64.
7. Jabbarpour, M.R.; Zarrabi, H.; Jung, J.J.; Kim, P. A green ant-based method for path planning of unmanned ground vehicles. *IEEE Access* **2017**, *5*, 1820–1832. [CrossRef]
8. Wang, Y.; Wang, X.; Fan, J.; Wang, Z.; Zhen, L. Emergency logistics network optimization with time window assignment. *Expert Syst. Appl.* **2023**, *214*, 119145. [CrossRef] [PubMed]
9. Moghdani, R.; Salimifard, K.; Demir, E.; Benyettou, A. The green vehicle routing problem: A systematic literature review. *J. Clean. Prod.* **2021**, *279*, 123691. [CrossRef]
10. Wang, J.; Yao, S.; Sheng, J.; Yang, H. Minimizing total carbon dioxide emissions in an integrated machine scheduling and vehicle routing problem. *J. Clean. Prod.* **2019**, *229*, 1004–1017. [CrossRef]
11. Niu, Y.; Yang, Z.; Chen, P.; Xiao, J. Optimizing the green open vehicle routing problem with time windows by minimizing comprehensive routing cost. *J. Clean. Prod.* **2018**, *171*, 962–971. [CrossRef]
12. Wang, Q.; Li, H.; Wang, D.; Cheng, T.C.E.; Yin, Y. Bi-objective perishable product delivery routing problem with stochastic demand. *Comput. Ind. Eng.* **2023**, *175*, 108837. [CrossRef]
13. Li, Y.; Soleimani, H.; Zohal, M. An improved ant colony optimization algorithm for the multi-depot green vehicle routing problem with multiple objectives. *J. Clean. Prod.* **2019**, *227*, 1161–1172. [CrossRef]
14. Anjum, S.S.; Noor, R.M.; Aghamohammadi, N.; Ahmedy, I.; Kiah, L.M.; Hussin, N.; Anisi, M.H.; Qureshi, M.A. Modeling traffic congestion based on air quality for greener environment: An empirical study. *IEEE Access* **2019**, *7*, 57100–57119. [CrossRef]
15. Laporte, G. Scheduling issues in vehicle routing. *Ann. Oper. Res.* **2016**, *236*, 463–474. [CrossRef]
16. Demir, E.; Bektas, T.; Laporte, G. An adaptive large neighborhood search heuristic for the Pollution-Routing Problem. *Eur. J. Oper. Res.* **2012**, *223*, 346–359. [CrossRef]
17. Ehmke, J.F.; Campbell, A.M.; Thomas, B.W. Vehicle routing to minimize time-dependent emissions in urban areas. *Eur. J. Oper. Res.* **2016**, *251*, 478–494. [CrossRef]
18. Zulvia, F.E.; Kuo, R.; Nugroho, D.Y. A many-objective gradient evolution algorithm for solving a green vehicle routing problem with time windows and time dependency for perishable products. *J. Clean. Prod.* **2020**, *242*, 118428. [CrossRef]

19. Ganji, M.; Kazemipoor, H.; Molana, S.M.H.; Sajadi, S.M. A green multi-objective integrated scheduling of production and distribution with heterogeneous fleet vehicle routing and time windows. *J. Clean. Prod.* **2020**, *259*, 120824. [CrossRef]
20. Asghari, M.; Al-e-hashem, S.M.J.M.; Afshari, H. Disruption management for the electric vehicle routing problem in a geographically flexible network. *Expert Syst. Appl.* **2023**, *214*, 119172. [CrossRef]
21. Vincent, F.Y.; Susanto, H.; Jodiawan, P.; Ho, T.W.; Lin, S.W.; Huang, Y.T. A simulated annealing algorithm for the vehicle routing problem with parcel lockers. *IEEE Access* **2022**, *10*, 20764–20782.
22. Huang, Y.X.; Zhao, L.; Woensel, T.V.; Gross, J.P. Time-dependent vehicle routing problem with path flexibility. *Transp. Res. Part B Methodol.* **2017**, *95*, 169–195. [CrossRef]
23. Zhao, F.; Si, B.; Wei, Z.; Lu, T. Time-dependent vehicle routing problem of perishable product delivery considering the differences among paths on the congested road. *Oper. Res.* **2023**, *23*, 5. [CrossRef]
24. Tan, K.; Liu, W.; Xu, F.; Li, C. Optimization Model and Algorithm of Logistics Vehicle Routing Problem under Major Emergency. *Mathematics* **2023**, *11*, 1274. [CrossRef]
25. Liu, R.; Jiang, Z. A constraint relaxation-based algorithm for the load-dependent vehicle routing problem with time windows. *Flex. Serv. Manuf. J.* **2019**, *31*, 331–353. [CrossRef]
26. Halassi Bacar, A.H.; Rawhoudine, S.C. An attractors-based particle swarm optimization for multi-objective capacitated vehicle routing problem. *RAIRO-Oper. Res.* **2021**, *55*, 2599–2614. [CrossRef]
27. Atasagun, G.C.; Karaoglan, I. A mathematical model for the time dependent vehicle routing problem with simultaneous pick-up and delivery. *J. Fac. Eng. Archit. Gazi Univ.* **2019**, *34*, 1743–1755.
28. Liu, P.; Wu, Z.; Shan, H.; Lin, F.; Wang, Q.; Wang, Q. Task offloading optimization for AGVs with fixed routes in industrial IoT environment. *China Commun.* **2023**, *20*, 302–314. [CrossRef]
29. Baker, B.M.; Ayechew, M.A. A genetic algorithm for the vehicle routing problem. *Comput. Oper. Res.* **2003**, *30*, 787–800. [CrossRef]
30. Liu, Q.; Xu, P.; Wu, Y.; Shen, T. A hybrid genetic algorithm for the electric vehicle routing problem with time windows. *Control. Theory Technol.* **2022**, *20*, 279–286. [CrossRef]
31. Pu, X.; Lu, X.; Han, G. An improved optimization algorithm for a multi-depot vehicle routing problem considering carbon emissions. *Environ. Sci. Pollut. Res.* **2022**, *29*, 54940–54955. [CrossRef]
32. Li, J.; Wang, D.; Zhang, J. Heterogeneous fixed fleet vehicle routing problem based on fuel and carbon emissions. *J. Clean. Prod.* **2018**, *201*, 896–908. [CrossRef]
33. Becker, C.; Gauthier, J.B.; Gschwind, T.; Schneider, M. In-depth analysis of granular local search for capacitated vehicle routing. *Discret. Appl. Math.* **2023**, *329*, 61–86. [CrossRef]
34. Brodal, G.S.; Jacob, R. Time-dependent networks as models to achieve fast exact time-table queries. *Electron. Notes Theor. Comput. Sci.* **2004**, *92*, 3–15. [CrossRef]
35. Chen, K.; Lei, Y.U. Microscopic traffic-emission simulation and case study for evaluation of traffic control strategies. *J. Transp. Syst. Eng.* **2007**, *7*, 93–99. [CrossRef]
36. Zhang, S.J.; Niu, T.L.; Wu, Y.; Zhang, K.M.; Wallington, T.J.; Xie, Q.; Wu, X.; Xu, H. Fine-grained vehicle emission management using intelligent transportation system data. *Environ. Pollut.* **2018**, *241*, 1027–1037. [CrossRef]
37. Sowden, M.; Cairncross, E.; Wilson, G.; Zunckel, M.; Kirillova, E.; Reddy, V.; Hietkamp, S. Developing a spatially and temporally resolved emission inventory for photochemical modeling in city of cape town and assessing its uncertainty. *Atmos. Environ.* **2008**, *42*, 7155–7164. [CrossRef]
38. Garaix, T.; Artigues, C.; Feillet, D.; Josselin, D. Vehicle routing problems with alternative paths: An application to on-demand transportation. *Eur. J. Oper. Res.* **2010**, *204*, 62–75. [CrossRef]
39. Liu, X.; Chen, Y.L.; Por, L.Y.; Ku, C.S. A systematic literature review of vehicle routing problems with time windows. *Sustainability* **2023**, *15*, 12004. [CrossRef]

Disclaimer/Publisher's Note: The statements, opinions and data contained in all publications are solely those of the individual author(s) and contributor(s) and not of MDPI and/or the editor(s). MDPI and/or the editor(s) disclaim responsibility for any injury to people or property resulting from any ideas, methods, instructions or products referred to in the content.